Catal Lett (2016) 146:2129–2138
DOI 10.1007/s10562-016-1814-6

Effect of Cu–Mo Activities on the Ni–Cu–Mo/Al_2O_3 Catalyst for CO_2 Reforming of Methane

Xumei Tao[1] · Guowei Wang[1] · Liang Huang[1] · Xiaoxiao Li[1] · Qingguo Ye[1]

Received: 16 March 2016 / Accepted: 12 July 2016 / Published online: 16 August 2016

Abstract A series of Ni–Cu–Mo/Al_2O_3 catalysts with different metal contents were prepared by sequential impregnation method. The performance of the catalysts for carbon dioxide reforming of methane was investigated in a quartz tubular reactor at CH_4/CO_2 ratio of 4/6, feed gas flux of 100 mL/min, catalysts 460 mg, temperature range of 600–900 °C and atmospheric pressure. The catalysts were characterized by XRD, XPS, BET, CO_2-TPD, TG, EDS and SEM. The performance and characterization results showed that the addition of Cu and Mo was beneficial for the reaction. The formation of spinel ($NiMoO_4$, $NiAl_2O_4$, $Cu_6Mo_4O_{15}$) and alloy (Ni_3Mo, $Cu_{3.8}Ni$) structures could significantly improve the catalytic activity and prevent the generation of carbon deposition. XRD patterns of the catalyst with the mass ratio of Ni:Mo = 0.75 after reaction suggested Mo_2C formation which could eliminate the coke and extend the stability. The catalyst with the mass ratio of Ni:Mo = 0.75 showed better activity and still remained highly active under the condition of 800 °C for 60 h. Therefore, the highly effective Ni–Cu–Mo/Al_2O_3 catalyst could be a potential catalyst for carbon dioxide reforming of methane.

Graphical Abstract

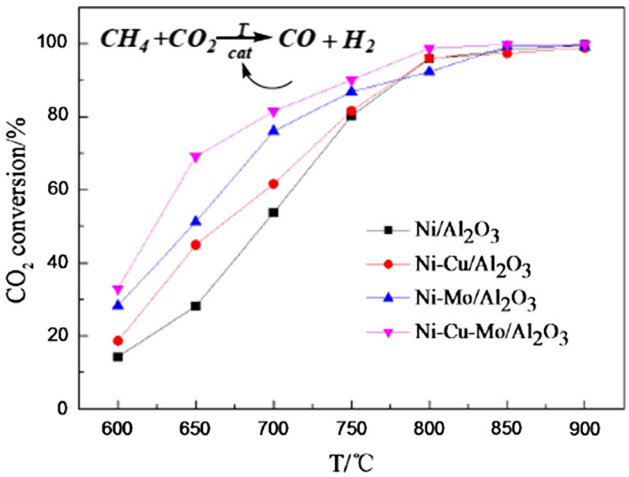

Keywords Carbon dioxide · Methane · Ni–Cu–Mo/Al_2O_3 catalyst · Ni:Mo mass ratio · Alloy

1 Introduction

Carbon dioxide reforming of methane has great potential and attracts many researchers' attention during recent years. It is of great significance because of the greenhouse effect, as well as energy and resource challenges. Nickel based catalysts have been extensively used in carbon dioxide reforming of methane due to relatively high activity and low cost, but sintering and carbon deposition over them prevent their application [1]. Improvement of nickel based catalysts is favorable.

To improve the performance of nickel based catalysts, various metallic active components were added into nickel

✉ Xumei Tao
qiqitxm_2002@sina.com.cn

[1] College of Chemical Engineering, Qingdao University of Science and Technology, Qingdao 266042, Shandong, China

based catalysts. Xinfa Dong et al. [2] investigated the effect of transition metal (Cu, Co and Fe) on the modification of nickel based catalysts for the autothermal reforming of methane. The results showed that the addition of transition metal Cu improved the dispersion of NiO, inhibited the formation of $NiAl_2O_4$, and thus significantly increased the activity of catalyst. Jae-Sung Choi et al. [3] studied CO_2 reforming of methane over modified Ni/Al_2O_3 catalysts. Catalysts modified with Cu showed slightly improved activity.

Moreover, investigations before had shown that Mo, as well as the oxides and carbides of Mo were excellent promoters to improve the performance of nickel based catalysts. The addition of Mo into nickel catalysts could effectively improve the metal-support interaction and lead to a decrease in carbon deposition [4–6]. The addition of MoO_3 enhanced the electron density of Ni and improved the stability of the catalysts [7]. Chuan Shi et al. [8] studied Ni-modified Mo_2C catalysts for methane dry reforming. Ni-Mo_2C was a typical bi-functional catalyst for methane dry reforming, and a catalytic redox cycle could be established by regulating the mass ratio of Ni and Mo_2C. The formation of the alloy between the active ingredients could basically eliminate carbon deposition on the catalyst and improve the catalytic performance of catalysts [9]. A. Djaidja [10] studied the Ni–M–Mg/Al (M = Fe or Cu) catalysts for CH_4–CO_2 reforming, the formation of Ni–Fe or Ni–Cu alloys led to a very good dispersion of the metal dispersion of the metal particles which explained the good catalytic stability observed in the CH_4-CO_2 reforming.

In the present work, Ni–Cu–Mo/Al_2O_3 catalyst was proposed for carbon dioxide reforming of methane. Comparing the properties and catalytic performance of Ni/Al_2O_3, Ni–Cu/Al_2O_3, Ni–Mo/Al_2O_3, Ni–Cu–Mo/Al_2O_3 catalysts, Ni–Cu–Mo/Al_2O_3 catalyst showed higher activity for the carbon dioxide reforming of methane reaction, affording high selectivity of CO and H_2.

2 Experimental

2.1 Catalyst Preparation

The 12 wt% Ni/Al_2O_3, Ni–Cu/Al_2O_3, Ni–Mo/Al_2O_3 and Ni–Cu–Mo/Al_2O_3 (Cu proportional content: 10 wt%) catalysts were prepared by impregnation method as shown in Fig. 1. γ-Al_2O_3 was first impregnated with aqueous solution of $(NH_4)_6Mo_7O_{24}{\cdot}H_2O$, and dried at 110 °C for 5 h, followed by calcination in a muffle furnace at 500 °C for 4 h to form MoO_3/Al_2O_3 compound. Trimetallic catalysts Ni–Cu–Mo/Al_2O_3 were prepared by impregnation of MoO_3/Al_2O_3 with mixtures of aqueous solutions of $Ni(NO_3)_2{\cdot}6H_2O$ and $Cu(NO_3)_2{\cdot}3H_2O$ in corresponding amount. Then, the catalysts were dried at 110 °C for 5 h, followed by calcination in a muffle furnace at 500 °C for 4 h and reduction at 700 °C for 2 h.

2.2 Catalytic Performance Tests

The catalytic performance tests were carried out in a quartz fixed-bed reactor at 600–900 °C. The feed mixture of 100 mL·min^{-1} with CH_4:CO_2 mol ratio of 4:6 was introduced into the reactor, and 460 mg of catalyst was charged in the reactor. The product composition was analyzed by an on-line gas chromatography (GC-1100) equipped with a TDX-01column (2 m × 3 mm) and with TCD detector (Fig. 2).

The conversions (X) of CH_4 and CO_2, the selectivity (S) of CO and H_2 were shown in form (1)–(4).

$$X(CH_4)\% = \frac{(F_{CH_{4,IN}} - F_{CH_{4,OUT}})}{F_{CH_{4,IN}}} \times 100\,\% \quad (1)$$

$$X(CO_2)\% = \frac{(F_{CO_{2,IN}} - F_{CO_{2,OUT}})}{F_{CO_{2,IN}}} \times 100\,\% \quad (2)$$

$$S(H_2)\% = \frac{F_{H_{2,OUT}}}{2 \times (F_{CH_{4,OUT}} - F_{CH_{4,IN}})} \times 100\,\% \quad (3)$$

$$S(CO)\% = \frac{F_{CO,OUT}}{[(F_{CH_4,IN} - F_{CH_4,OUT}) + (F_{CO_2,IN} - F_{CO_2,OUT})]} \times 100\,\% \quad (4)$$

2.3 Catalyst Stability Test

The reforming reaction was carried out at 800 °C for 80 h in order to study the long term stability of the catalyst with Ni:Mo mass ratio of 0.75. The feed mixture of 100 mL min^{-1} with CH_4:CO_2 mol ratio of 4:6 was introduced into the reactor, and 460 mg of catalyst was charged in the reactor.

2.4 Catalyst Characterization

X-ray diffraction (XRD) of the catalysts was recorded with an X-ray diffractometer (RINT2000, Japan) using monochromatic Cu Kα radition at 40 kV and 150 mA. The diffraction patterns were recorded in the 2θ range of 10–80° with a scanning speed of 10°min^{-1} and a step size of 0.02°s^{-1}. X-ray photoelectron spectra (XPS) was measured on an Thermo ESCALAB 250Xi (US) spectrometer using monochromatized Al Kα radiation at electron gun power of 150 W, and the Al Kα monochromatized line

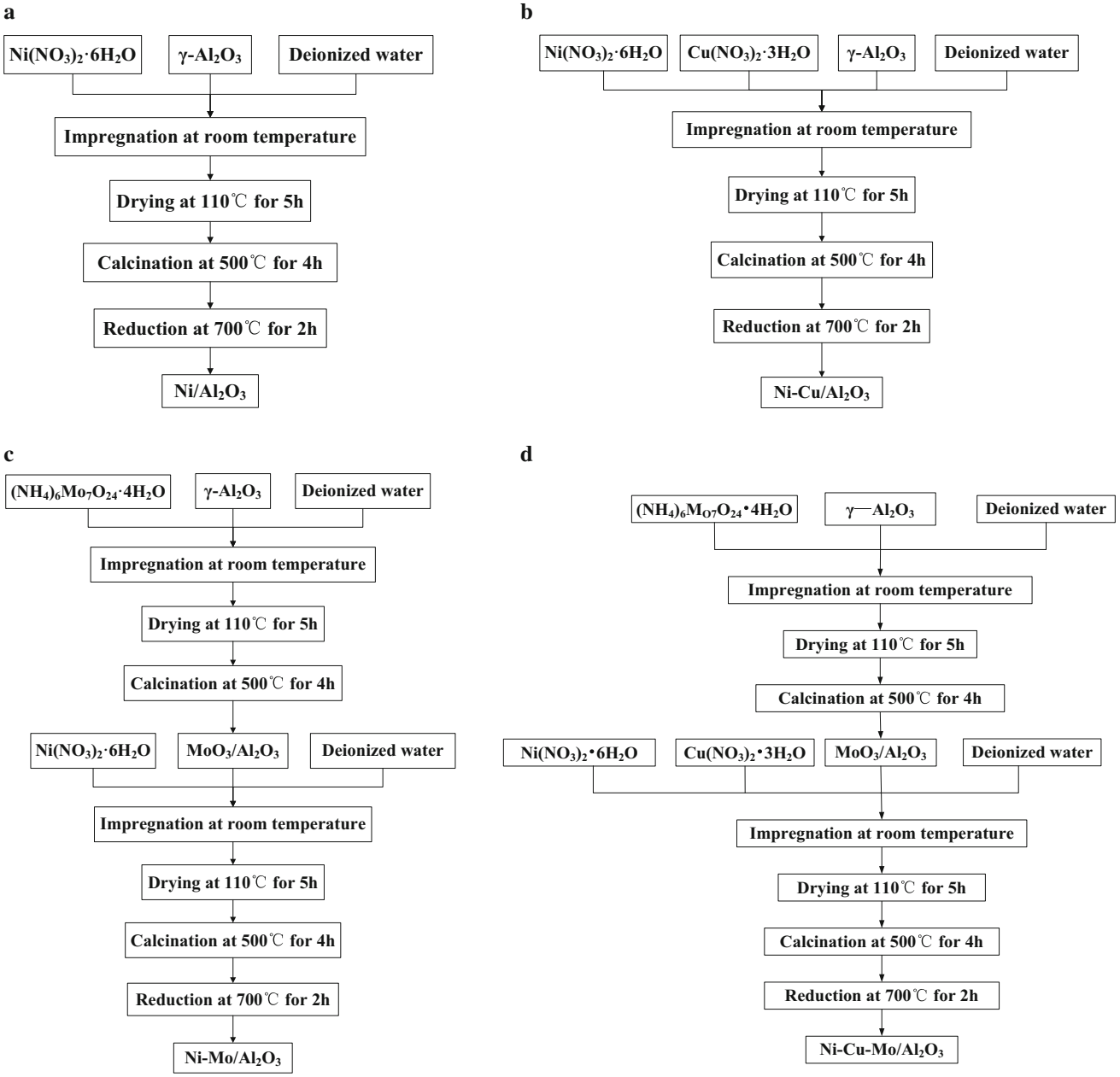

Fig. 1 Schematic flow chart for the preparation steps of the four kinds of the catalysts

(1486.6 eV) was adopted during the analysis. The BET surface area measurements were performed with N_2 adsorption at −196 °C using an adsorption unit ASAP2020. CO_2 temperature-programmed desorption (CO_2-TPD) was performed on an AutoChemII 2920 Analyzer. 400 mg of catalyst was heated to 350 °C and kept for 60 min in Ar stream. Then, the catalyst was cooled down to ambient temperature and followed by adsorption with pure CO_2. After adsorption, the catalyst was purged with He stream. The desorption of CO_2 was carried out with a heating rate of 6 °C·min^{-1} to 500 °C and measured by a mass spectrometer. Scanning electron microscope (SEM) images were carried out with a JSM-6700F instrument operated at 8 kV. The thermal analyses were carried out on a NETZSCH TG/209/F1 thermoanalyzer. The measurements were conducted in dynamic air atmosphere (50 mL min^{-1}), using the alumina plates crucibles of 150 mL. The heating rate was of 20 K min^{-1} in the range of temperature 30–900 °C and the mass samples were about 4 mg. Energy Dispersive Spectroscopy (EDS) was also used for qualitative detection of Ni, Cu, Mo elements in the catalyst matrix.

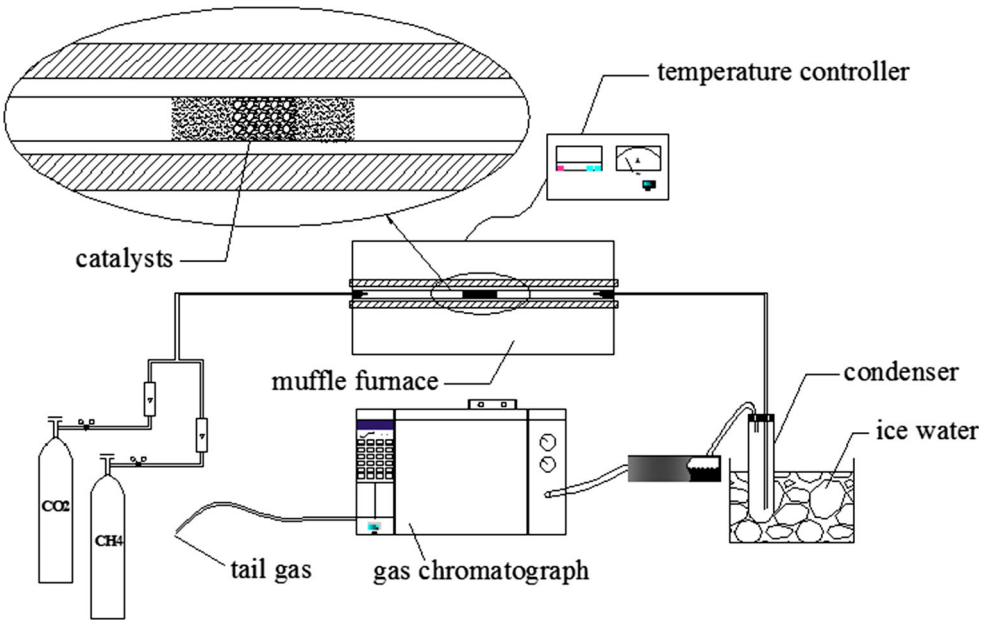

Fig. 2 Schematic flow chart for carbon dioxide reforming of methane

3 Results and Discussion

3.1 Catalytic Performance

The Ni content 12 wt% with the Ni/Al_2O_3, $Ni\text{-}Cu/Al_2O_3$, $Ni\text{-}Mo/Al_2O_3$, $Ni–Cu–Mo/Al_2O_3$ catalytic performances for carbon dioxide reforming of methane were shown in Fig. 3, which showed the reactants conversion as a function of temperature. From the results, it was apparent that the catalytic activities of four kinds of catalysts were presented the same trend, namely the reactants conversion increased significantly with increasing temperature. In fact, the increase in catalytic performance with temperature conformed to the thermodynamics of the process since it was an endothermic reaction. The Ni/Al_2O_3 catalyst conversion rate was the lowest. The conversion rates of the $Ni–Cu/Al_2O_3$ and $Ni\text{-}Mo/Al_2O_3$ were similar and higher and the conversion rate of the $Ni–Cu–Mo/Al_2O_3$ was the highest. This showed that on the basis of Ni catalysts added Cu or Mo fertilizer could enhance the catalytic activity of catalysts, adding the two Cu and Mo fertilizers could further increase the catalytic activity of the catalysts, especially at low temperatures (650–750 °C). The reason may be that between Ni and Cu or Mo formed some kinds of new structure and this could be achieved by characterization of catalysts.

Figure 4 illustrated the catalytic performance of the $Ni–Cu–Mo/Al_2O_3$ catalyst with the different Ni:Mo mass ratio for carbon dioxide reforming of methane, showing the reactants conversion and products selectivity as a function of temperature. From the results, it was apparent that the reactants conversion increased with increasing temperature, while there was negligible difference in products selectivity. In 600–800 °C temperature range, the

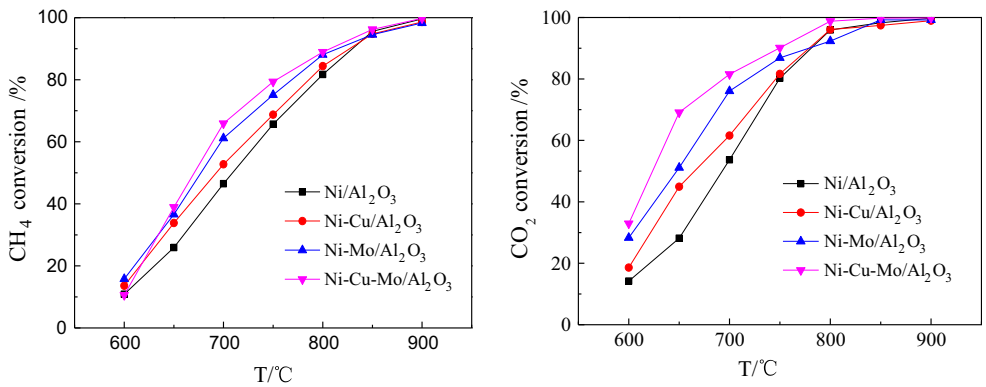

Fig. 3 Four catalytic performances for carbon dioxide reforming of methane

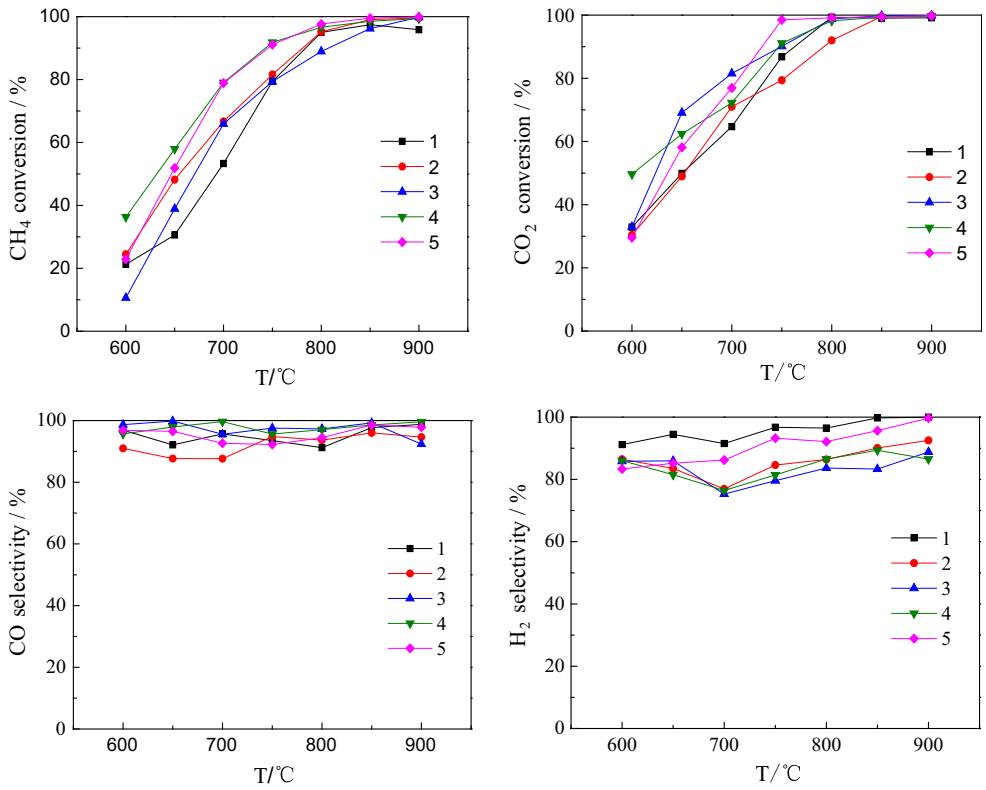

Fig. 4 Catalysis activities of the Ni–Cu–Mo/Al_2O_3 with different Ni/Mo mass ratio. *1* Ni:Mo = 0.15; *2* Ni:Mo = 0.30; *3* Ni:Mo = 0.45; *4* Ni:Mo = 0.60; *5* Ni:Mo = 0.75

conversions increased rapidly with the increase of reaction temperature. But as the temperature increased, the conversion rate increased slower. When temperature was higher than 750 °C, as the temperature increased, the conversion rates basically remained unchanged. Therefore, the proper temperature for the Ni–Cu–Mo/Al_2O_3 catalysts was 750 °C. The reactants conversion and products selectivity also varied with the Ni:Mo mass ratio. The catalyst with the mass ratio of Ni:Mo = 0.75 showed higher activities. The conversions of CH_4 and CO_2 reached 97.68 and 99.12 %, and the selectivity of CO and H_2 reached 92.96 and 90.01 % at 800 °C, respectively.

3.2 Catalyst Stability

Figure 5 illustrated the stability of the catalyst with the mass ratio of Ni:Mo = 0.75. The stability of the catalyst was tested in the quartz fixed-bed reactor at 800 °C. As to the catalyst with Ni:Mo mass ratio of 0.75, the conversions of methane and carbon dioxide were over 90 %, and the conversions still remained at 90 % till 60 h. The Reaction conversion rate after 60 h began to gradually reduce. This showed that the Ni–Cu–Mo/Al_2O_3 catalyst was highly active.

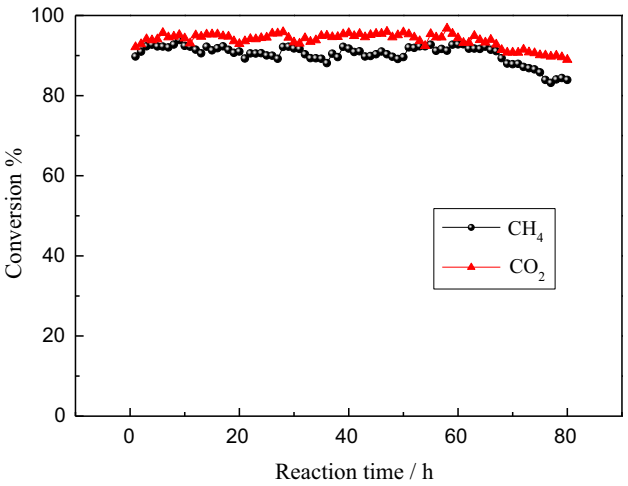

Fig. 5 The stability of the catalyst with the mass ratio of Ni:Mo = 0.75

3.3 Catalyst Characterization

Figure 6 showed the XRD patterns in the range of 10–80° of the catalysts with different mass ratio of Ni:Mo. It appeared that nickel was mainly in the form of elemental distribution in the catalyst, a few in the form of spinel

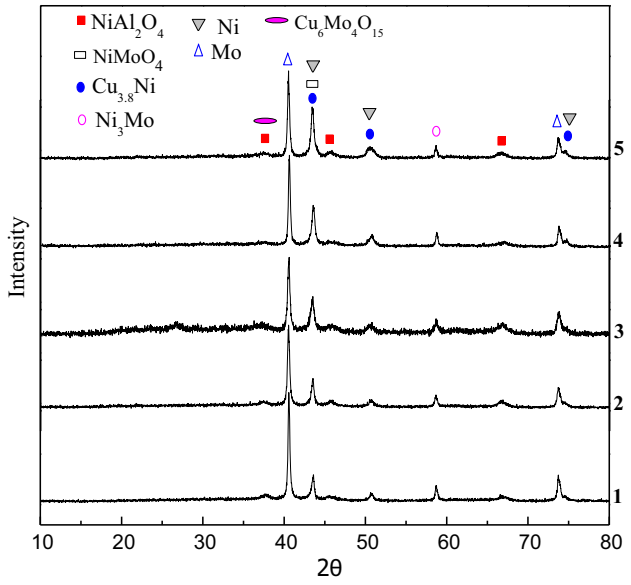

Fig. 6 XRD patterns of Ni–Cu–Mo/Al_2O_3 catalysts with different mass ratio of Ni:Mo. *1* Ni:Mo = 0.15; *2* Ni:Mo = 0.30; *3* Ni:Mo = 0.45; *4* Ni:Mo = 0.60; *5* Ni:Mo = 0.75

($NiAl_2O_4$) or alloy (Ni_3Mo, $Cu_{3.8}Ni$) and the Cu or Mo additives formed the $Cu_6Mo_4O_{15}$ metal oxides. The structures of $NiMoO_4$ and $NiAl_2O_4$ could effectively prevent the sintering of nickel and improve the activity of catalysts. The broadness of Ni_3Mo and $Cu_{3.8}Ni$ characteristic peaks increased with the increasing mass ratio of Ni:Mo. The $NiMoO_4$ characteristic peak of the catalyst with Ni:Mo mass ratio of 0.75 was high and sharp, which explained that the crystal shape was perfect. The characteristic peaks of the alloy Ni_3Mo and $Cu_{3.8}Ni$ were wide and low, suggesting that the formation of the grain size was small and the dispersion was high. It suggested that the alloy structure formed between Ni and Cu or Mo could significantly improve the catalytic activity of catalysts, which was consistent with the results of the catalytic performance tests. The Ni surface area and average Ni particle size as shown in Table 1 were calculated according to the method described in Ref. [11].

Figure 7 Showed the XRD patterns of Ni–Cu–Mo/Al_2O_3 catalyst with the mass ratio of Ni/Mo = 0.75 after reaction.

Table 1 Ni dispersion on Ni–Cu–Mo/Al_2O_3 catalyst

Catalysts	Ni diameter (nm)	Ni surface area (m^2/g-Ni)
Ni:Mo = 0.15	23.7	33
Ni:Mo = 0.30	27.7	28
Ni:Mo = 0.45	23.2	34
Ni:Mo = 0.60	21.1	37
Ni:Mo = 0.75	19.5	40

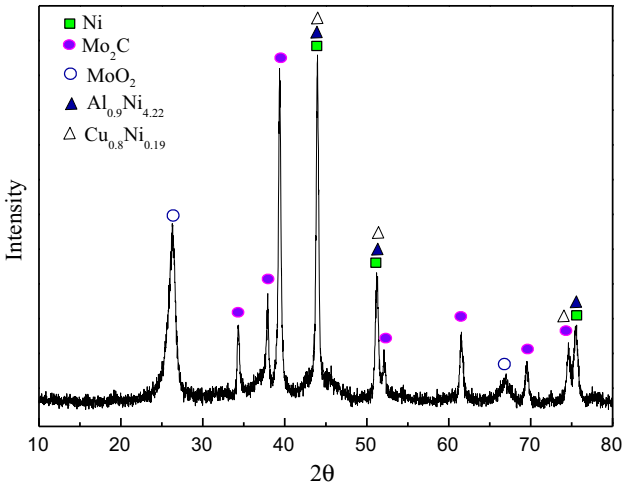

Fig. 7 XRD patterns of Ni–Cu–Mo/Al_2O_3 catalyst with the mass ratio of Ni/Mo = 0.75 after reaction

The spinel and alloy structures disappeared after reaction, while MoO_2, Mo_2C, $Al_{0.9}Ni_{4.22}$ and $Cu_{0.8}Ni_{0.19}$ species formed. The results suggested that the addition of Cu and Mo induced strong metal-support interaction, which was reported as one of the contributions to good catalytic performance [12]. Mo_2C, which was also catalytically active for carbon dioxide reforming of methane, contributed to the prevention of carbon deposition and extended the stability of the catalyst.

X-ray photoelectron measurements were performed over the Ni–Cu–Mo/Al_2O_3catalyst with Ni:Mo mass ratio of 0.75 to investigate the surface properties and elemental oxidation states. Figure 8 showed the XPS patterns of the catalyst with Ni:Mo mass ratio of 0.75, and the Al Kα monochromatized line (1486.6 eV) was adopted during the analysis. The samples were pressed into a thin pellet, and the binding energys (BEs) were corrected with the reference BE of C1 s (284.6 eV).

The spectra of Ni2p, Cu2p, Mo3d, Al2p, O1 s were taken at the constant analyzer energy mode (30 eV pass energy) and C1 s at the 50 eV pass energy. XPS analysis was performed to examine the elemental composition and to determine the valence state of elements of the catalysts. For the O1 s spectra, the O1 s peak is generally complicated because of the O ions from different oxides. As per the literature, the O^{2-} was existed in CeO_2 at the peak of 529.6 eV [13]. And the O1 s binding energy value reported for Rh_2O_3 was 530.0 eV [14]. On this basis, the peak at 529.87 eV may be attributed to O^{2-} of the $NiAl_2O_4$, $NiMoO_4$ and $Cu_6Mo_4O_{15}$. The BEs of Al2p on the Ni/Al_2O_3 catalysts were found to be in the range of 73.7–74.1 eV without significant variations [15], which suggested the Al^{3+} of the formation of spinel $NiAl_2O_4$ species. For the Ni2p spectra, Ni mainly existed as Ni^0

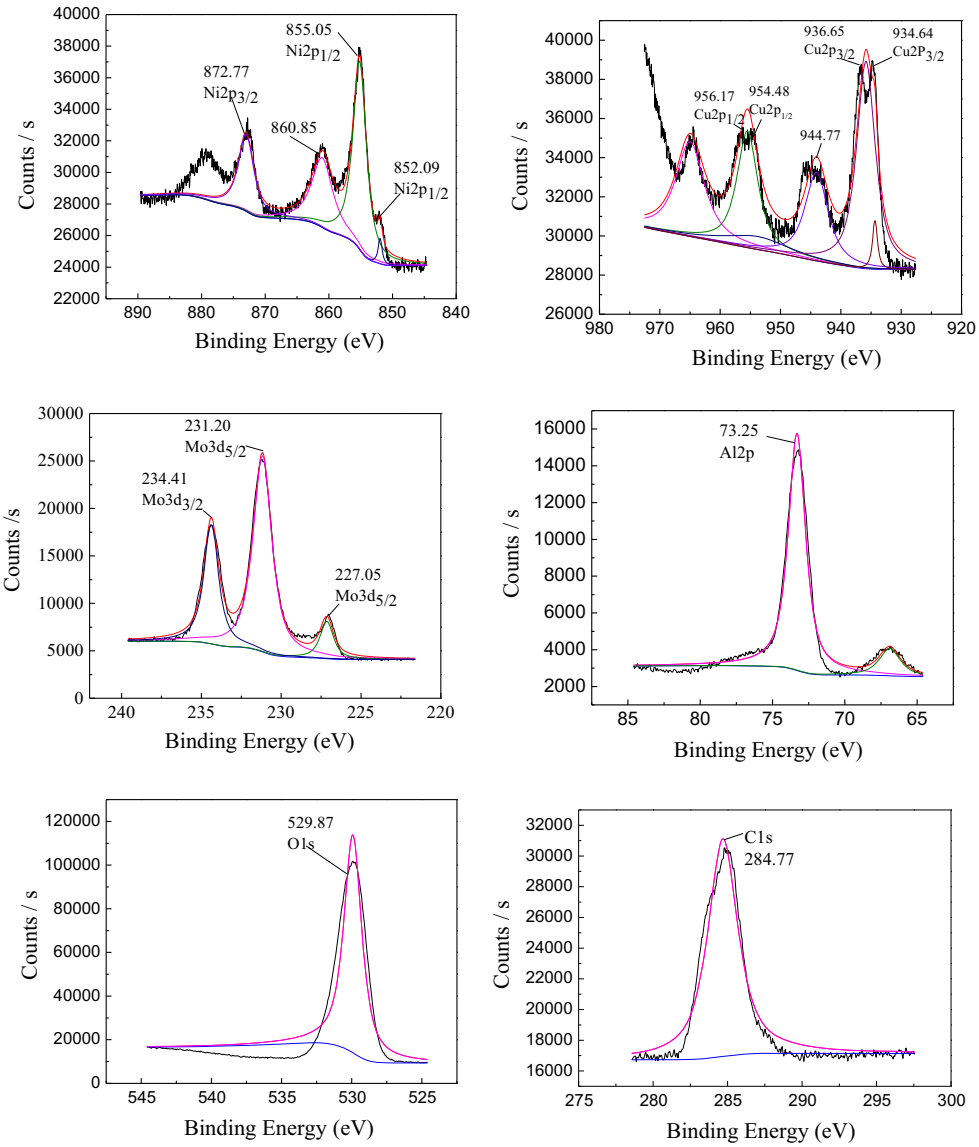

Fig. 8 XPS patterns of Ni–Cu–Mo/Al_2O_3 catalyst with Ni:Mo mass ratio of 0.75

(852.48 ± 0.5 eV) in Zr-based catalyst [16] and Ni^0 (852.7 eV) in Ni–Co catalyst [17]. Ni mainly existed as Ni^{2+} (853.5–855.6 eV) [18] or (856 or 874 eV) [19]. As it is shown in Fig. 8, the low-intensive peak of 852.06 eV could be assigned to Ni elemental. The peak of 852.06 and 872.74 eV were attributed to Ni^{2+}, which may be the spinel $NiAl_2O_4$ or the $NiMoO_4$. In addition, the higher energy peak (860.85 eV) may be associated with the Ni_3-Mo or $Cu_{3.8}Ni$ alloy, which combined with the XRD analysis. By the peak intensity, it could also find that the more the alloy component content, the better the CH_4 and CO_2 conversions. The observed binding energy values for various Mo phases differ from the one reported in the Ref. [19] and the BEs were performed Mo^0 (227.9–228.2 eV), Mo^{4+} (229.4–229.6 eV) and Mo^{6+} (232.5–232.6 eV) [19]. We could speculate that the peak of 227.52 eV was the metal state Mo^0 (which was consistent with the results of XRD). The 234.41 eV may be Mo^{6+} existed in the $NiMoO_4$ and the 231.2 eV may be the Ni_3Mo alloy structure. Due to the different chemical environment of the Cu element, the observed binding energy values for various Cu phases were very complex. The satellite peak at 940–950 eV was the copper oxide [20]. The peak at 932.4 and 934.3 eV could be attributed to presence of Cu^{1+} and Cu^{2+}, respectively [21]. The binding energies at 952.2 and 932.3 eV can be attributed to Cu^0 and Cu^{1+}, respectively [22]. From the XRD analysis, we could know that the Cu element existed in the $Cu_6Mo_4O_{15}$ metal oxides and the $Cu_{3.8}Ni$ alloy. Due to the Ni^{2+}, Mo^{6+}, Al^{3+}, O^{2-}, the valence state of the Cu element should be Cu^{1+}. On this

basis, the peak at 944.74 and 954.48 eV may be the $Cu_6Mo_4O_{15}$ metal oxides. The higher-intensive BEs (934.64 and 936.65 eV) may be attributed to $Cu_{3.8}Ni$ alloy.

On the one hand, the $NiAl_2O_4$, $Cu_6Mo_4O_{15}$ and $NiMoO_4$ played a fixed role for the active components; on the other hand, they also provided the oxygen in the process of the reaction to prevent the generation of carbon deposition. Since the presence of the metal alloys could increase the dispersion of the active components, the existence of Ni_3Mo and $Cu_{3.8}Ni$ alloy could also improve the catalytic activity of the Ni–Cu–Mo/Al_2O_3 catalyst.

Figure 9 presented the SEM images of Ni–Cu–Mo/Al_2O_3 catalysts with different mass ratio of Ni:Mo. The images showed that the metals dispersed uniformly on the support.

Table 2 showed the surface and pore properties of Ni–Cu–Mo/Al_2O_3 catalysts with different mass ratio of Ni:Mo. The BET surface area, average pore diameter and pore volume did not vary much between Ni–Cu–Mo/Al_2O_3 catalysts with different mass ratio of Ni:Mo. The catalyst with Ni:Mo mass ratio of 0.75 exhibited the biggest BET surface area, which might be favorable for the catalytic reaction.

The CO_2-TPD curves of Ni–Cu–Mo/Al_2O_3 catalysts with different mass ratio of Ni:Mo were presented in Fig. 10. It was apparent from TPD profiles that all catalysts

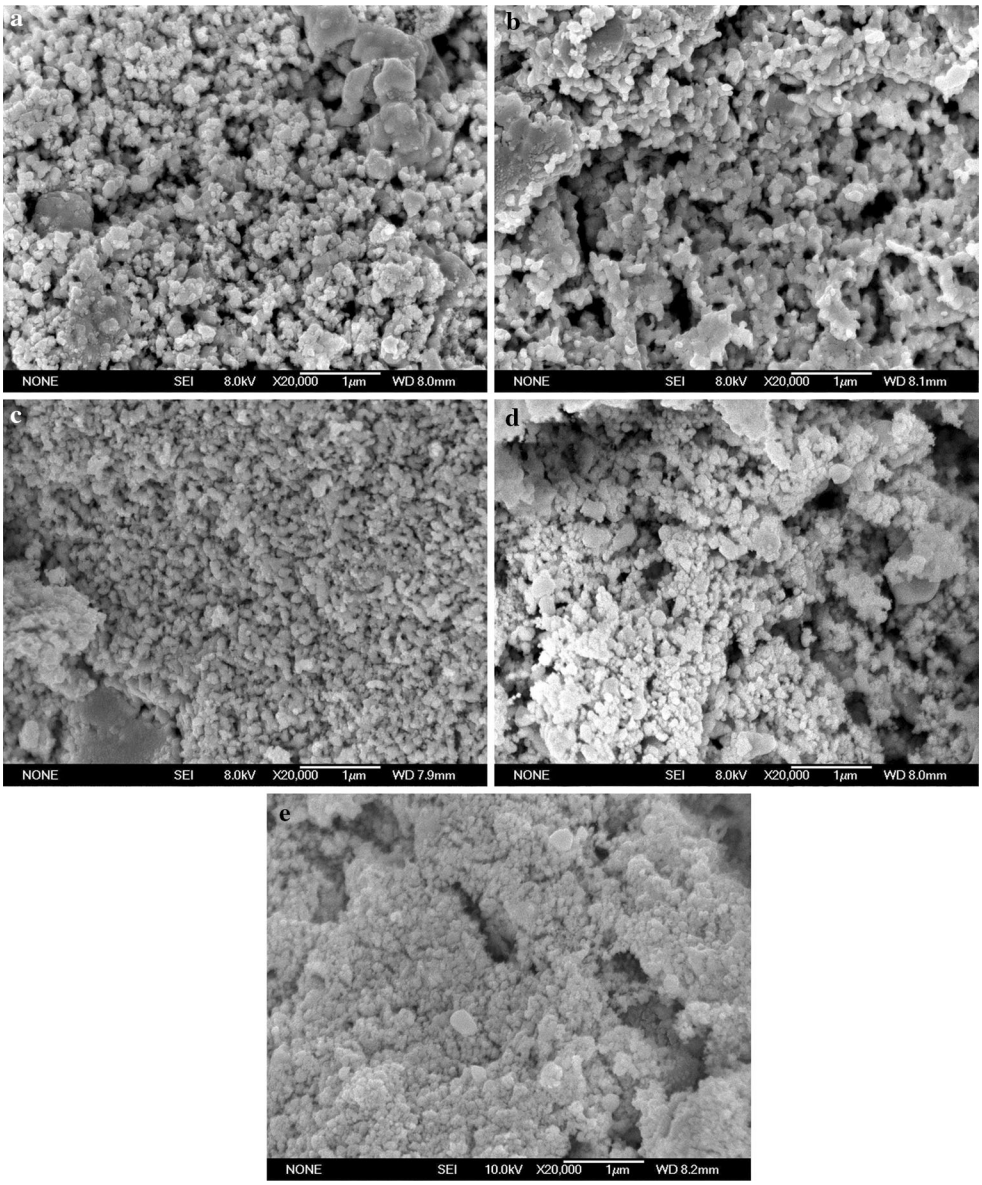

Fig. 9 SEM images of Ni–Cu–Mo/Al_2O_3 catalysts with different mass ratio of Ni:Mo **a** Ni:Mo = 0.15; **b** Ni:Mo = 0.30; **c** Ni:Mo = 0.45; **d** Ni:Mo = 0.60; **e** Ni:Mo = 0.75

Table 2 The surface and pore structure of Ni–Cu–Mo/Al_2O_3 catalysts

Catalysts	BET surface area (m^2 g^{-1})	Average pore diameter (nm)	Pore volume (cm^3 g^{-1})
Ni:Mo = 0.15	59	15	0.24
Ni:Mo = 0.30	60	14	0.23
Ni:Mo = 0.45	63	12	0.20
Ni:Mo = 0.60	53	13	0.18
Ni:Mo = 0.75	65	13	0.22

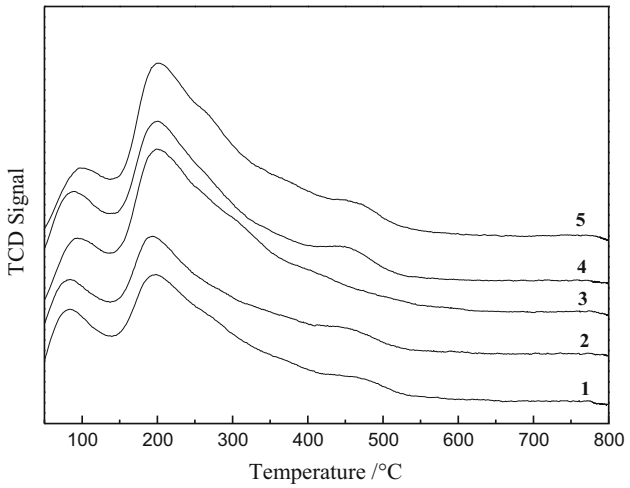

Fig. 10 CO_2-TPD patterns of Ni–Cu–Mo/Al_2O_3 catalysts with different mass ratio of Ni:Mo *1* Ni:Mo = 0.15; *2* Ni:Mo = 0.30; *3* Ni:Mo = 0.45; *4* Ni:Mo = 0.60; *5* Ni:Mo = 0.75

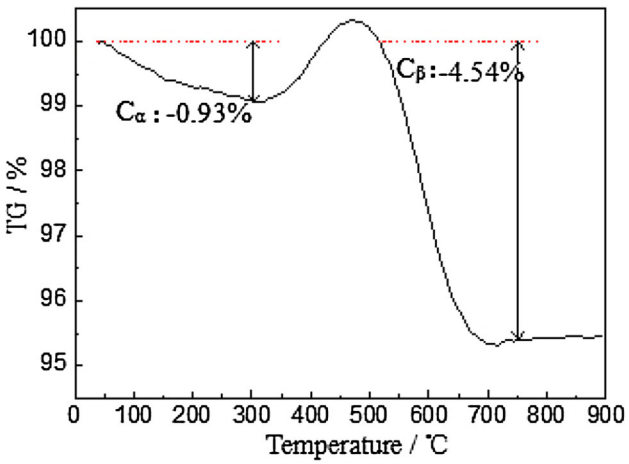

Fig. 11 TG analysis of Ni–Cu–Mo/Al_2O_3 catalyst after reaction with the mass ratio of Ni:Mo = 0.75

showed three CO_2 desorption peaks at about 100, 200 and 450 °C, respectively. The research estimated that the CO_2 adsorbed on weaker sites was desorbed at low temperature while that adsorbed on strong sites was desorbed at high temperature [23]. The increase in Ni:Mo mass ratio led to the increase in peak areas toward high temperature, which were assigned to medium and strong sites.

In order to further verify the Ni–Cu–Mo/Al_2O_3 catalyst with the Ni/Mo ratio of 0.75 could simultaneously lead to both high stability and high activity, the catalyst was tested in the same reaction for 80 h at the 800 °C.

Zhang et al. [24] found that on the surface of Ni/Al_2O_3 catalyst there were three forms of carbon deposition: the surface of the catalyst was mainly C_α at 150–220 °C, which was a kind of active carbon mainly responsible for generating the syngas; At 500–600 °C, the catalyst surface were mainly C_β, which may be involved in generating CO at more than 600 °C; When temperature greater than 650 °C, the catalyst surface mainly existed in the form of C_γ, which was the main factor that led to the catalyst deactivation. Figure 11 showed the TG analysis of the Ni–Cu–Mo/Al_2O_3 catalyst which reacted in CH_4–CO_2 reforming reaction at 800 °C for 80 h. Figure 11 suggested that the amount of carbon deposition C_α and C_β were 1.17 and 51.57 %, respectively. And the C_γ was not found in the catalyst after reaction. Since the C_γ was the main factor that led to the catalyst deactivation, the absent of C_γ may be the reason for high catalytic stability of the Ni–Cu–Mo/Al_2O_3 catalyst for CH_4–CO_2 reforming reaction at 800 °C after 80 h. TG analysis further verified the existence of the alloy structure may inhibit carbon deposition.

The EDS quantitative analysis was carried out on the catalyst surface element and the relative contents of surface Ni, Cu and Mo were obtained for Ni–Cu–Mo/Al_2O_3 catalyst with the Ni/Mo ratio of 0.75. Data results as shown in Table 3 indicated that Ni–Cu–Mo/Al_2O_3 catalyst had good dispersion which could promote the reaction.

Table 3 Final composition of Ni–Cu–Mo/Al_2O_3 catalyst with Ni:Mo mass ratio of 0.75

Element	EDS wt%
Ni	13.00
Cu	9.56
Mo	17.30

4 Conclusions

With the addition of Cu and Mo, a series of Ni–Cu–Mo/Al_2O_3 catalysts with different mass ratio of Ni:Mo were prepared and applied for CH_4–CO_2 reforming. The spinel ($NiMoO_4$, $NiAl_2O_4$, $Cu_6Mo_4O_{15}$) and alloy (Ni_3Mo, $Cu_{3.8}Ni$) structures were formed. The chemical composition of the Ni–Cu and Ni–Mo alloys were found to have a higher dispersed state in the Ni–Cu–Mo/Al_2O_3 catalyst. The Ni–Cu–Mo/Al_2O_3 catalysts had high BET surface area and uniform distribution, and showed potential for carbon dioxide reforming of methane. The formation of Mo2C after reaction contributed to the prevention of carbon deposition and high stability of the catalyst.

Acknowledgments Financial supports from Shandong Excellent Young Scientists Fund (BS2011NJ006) are acknowledged.

References

1. Nader R, Mohammad H, Ali AB, Somaiyeh A, Mahdi FJ (2014) Energy Convers Manag 84:50–59
2. Dong XF, Cai XL, Song YB, Lin WM (2007) J Nat Gas Chem 16(1):31–36
3. Choi JS, Moon KI, Kim YG, Lee JS, Kim CH, David L (1998) Catal Lett 52(1–2):43–47
4. Huang T, Huang W, Huang J, Ji P (2011) Fuel Process Technol 92(10):1868–1875
5. Quincoces CE, Vargas SP, Grange P, Gonzźlez MG (2002) Mater Lett 56(5):698–704
6. Borowiecki T, Gac W, Denis A (2004) Appl Catal A 270(1–2):27–36
7. Liu HT, Tian H, Wang XL (2007) J Mol Catal (China) 21(4):304–307
8. Shi C, Zhang AJ, Li XS, Zhang SH, Zhu AM, Ma YF, Au CT (2012) Appl Catal A 431–432:164–170
9. Chen L, Hao ZD, Yang TZ (2014) Int J Hydrogen Energy 39:15474–15481
10. Djaidja A, Messaoudi H, Kaddeche D (2015) Int J Hydrogen Energy 40(14):4989–4995
11. Donald DG, Bartholomew CH (1981) J Catal 67:186–206
12. Wang SB, Lu GQM (1988) Appl Catal B 16(3):269–277
13. Reddy BM, Rao KN, Reddy GK, Khan A, Park SE (2007) J Phys Chem C 11(50):18751–18758
14. Sheerin E, Reddy GK, Smirniotis P (2016) Catal Today 263:75–83
15. Lee HY, Kim AR, Park MJ, Jo JM, Lee DH, Bae JW (2015) Chem Eng J 280:771–781
16. Survilienè S, Cešūnienė A, Jasulaitienė V, Jureviciūte I (2012) Appl Surf Sci 258:9902–9906
17. Jian Li.(2014) Studies on Stability and Coke-Resistant properties of CoNi Alloy Catalysts for Dry Reforming [D].East China University of Science and Technology.
18. Ivanova TM, Kochur AG, Maslakov KI, Kiskin MA, Savilov SV, Lunin VV, Novotortsev VM, Eremenko IL (2015) J Electron Spectrosc Relat Phenom 205:1–5
19. Kukushkin RG, Bulavchenko OA, Kaichev VV, Yakovlev VA (2015) Appl Catal B 163:531–538
20. Zhao J, Li YX, Zhu YQ, Wang Y, Wang CY (2015) Appl Catal A 510:34–41
21. Rahemi N, Haghighi M, Babaluo AA (2014) Energy Convers Manag 84:50–59
22. Sato AG, Volanti DP, Meira DM, Damyanova S, Longo E (2013) J Catal 307:1–17
23. Naeem MA, Al-Fatesh AS, Abasaeed AE, Fakeeha AH (2014) Fuel Process Technol 122:141–152
24. Tsipouriari VA, Efstathiou AM, Zhang ZL, Verykios XE (1994) Catal Today 21(2–3):589–595